Getting Something from Almost Nothing by Supervirtual Interferometry

Kai Lu[1], Sherif Hanafy[1] and Gerard Schuster[1]
[1] King Abdullah University of Science and Technology, Division of Physical Science and Engineering, Thuwal 23955-6900. Saudi Arabia

ABSTRACT

We recently collected refraction data over a windy site in East Africa. Almost 60% of the first arrivals at intermediate-to-long offsets were unpickable due to heavy wind noise and strong near-surface scattering. Bandpass filtering and prediction-error filtering was inadequate in extracting pickable events from the noise. However, the application of supervirtual interferometry to these data allowed us to recover nearly 90% of the unpickable data.

INTRODUCTION

Estimating the subsurface velocity distribution by inverting refraction traveltimes is one of the most widely used imaging methods in seismology. It can be used to invert the traveltimes of teleseisms for the crust and mantle velocity model, which is essential for understanding the tectonics of Earth (Sheriff and Geldart, 1995). Refraction tomography from controlled source experiments is also used to estimate the initial starting model for full waveform inversion (Tarantola, 1984) as well as for estimates of basin depth and near-surface velocity anomalies. Identifying the location of near-surface velocity anomalies is important for estimating statics (Zhu et al., 1992) and earthquake hazards (Morey and Schuster, 1999), and assessing geohazard sites for the construction of dams, buildings, and roads.

SVI PROCEDURE

One of the problems with refraction imaging using controlled-source data is that the signal-to-noise ratio (SNR) diminishes with offset between the source and receivers. The consequence is that accurate traveltime picking is not possible beyond a critical offset and so severely limits the use of refraction imaging with affordable sources. For example, an offset of more than 4 km is typically needed to reach the depth of 1 km for a land survey[1].

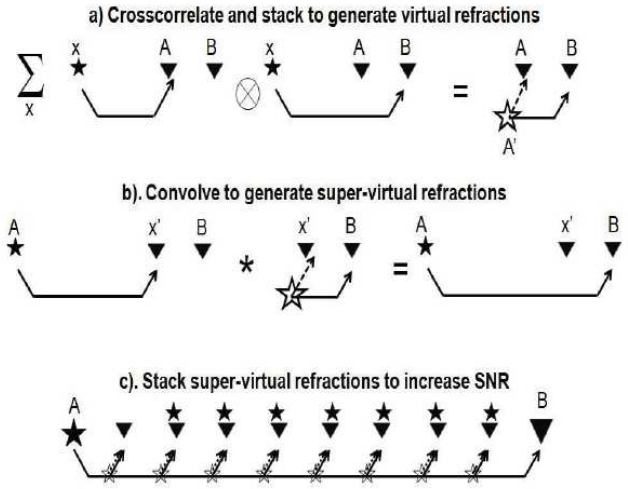

Figure 1: Illustration of SVI procedures. Dashed arrows in a) and b) indicate negative times from the star to the receiver while solid lines indicate positive traveltimes.

To partly mitigate this problem, refraction interferometry (Dong et al., 2006; Mallinson et al., 2011; Nichols et al., 2010) was developed to enhance the signal-to-noise ratio of refraction arrivals. The key idea is illustrated in Figure 1(a) where two traces can be correlated with one another for any post-critical source, and the resulting correlograms have the correlated refraction event now arriving at the same time for any post-critical source. If there are N_s post-critical sources then the stacked correlograms increase the signal-to-noise ratio by $\sqrt{N_s}$. This

[1]For land surveys, an offset-to-depth ratio well over 4:1 is required to obtain the refraction arrival from the depth of interest.

SNR can be further increased by using supervirtual interferometry (Bharadwaj et al., 2013) where the virtual sources at depth in Figure 1(a) can be redatumed to be on the surface again. This redatuming is carried out by convolving the virtual trace at **B** in Figure 1(a) with the recorded trace at $\mathbf{x}'$ in Figure 1(b) to give the supervirtual trace at **B** in Figure 1(b). The resulting refraction arrival will arrive at the same time for any post-critical trace between the geophone at **B** and the source position; hence stacking over these supervirtual traces will enhance the SNR by an additional $\sqrt{N_r}$, where N_r is the number of postcritical receivers offset from the source. Thus the final SNR of the supervirtual trace can be enhanced by as much as $\sqrt{N_r + N_s}$, and this procedure is denoted as supervirtual interferometry (SVI).

This enhancement can be even greater because the correlation operation acts like a matched filter that suppresses random noise. An additional SNR enhancement can sometimes be achieved by iteratively repeating the SVI procedure, where the input data are the SVI traces from the previous iteration (Al-Hagan et al., 2014).

The SVI procedure has only recently been developed and so there are many untested applications. A large offset marine application was successfully tested by Bharadwaj et al. (2012) for source-receiver offsets out to more than 80 km, and it was also tested for imaging a Nevada basin where the SNR of far-offset arrivals was poor, but still faintly visible (Mallinson et al., 2011). Will SVI work well when the far-offset arrivals are invisible to the naked eye? This paper answers this question for refraction data where both the intermediate and far-offset arrivals are mostly undetectable by the human eye. In other words, SVI can significantly enhance the SNR of refraction arrivals for refraction data when it appears that there is almost nothing at most offsets.

The next section demonstrates SVI imaging on an extremely noisy refraction data set, and is followed by the conclusions.

The SVI procedure consists of the following steps:

1. Window about the target refractions.
2. Cross-correlate raw trace pairs to generate virtual refractions.
3. Stack virtual refractions associated with the same receiver locations to improve the SNR.
4. Convolve virtual traces with raw traces to generate super-virtual refractions.
5. Stack super-virtual refractions with the same source and receiver locations to improve the SNR.
6. The SVI output can be used as the input to further iterations to improve the SNR.

The key step for a successful implementations of SVI is proper windowing, which is especially tricky when the target refractions are almost invisible. The ideal case is to pick a window that only contains the target event, which is nearly impossible. More practically, a window containing both the target event, as well as some other events which are not significantly stronger than our target, is acceptable. To deal with a noisy dataset, preprocessing steps such as bandpass filtering and amplitude balancing are required for a less noisy view of the first arrival, and make windowing easier. At the far-offset where the first arrival is almost invisible, we window by predicting the rough position of the refraction arrivals. The apparent velocity of the visible part of the first arrivals and the neighbouring common shot gathers both can be used to assist this prediction. A window that is several periods tall is suggested for the first trial where the target refractions are likely to be extant. Then we use the SVI output of the trial windows as a reference to further adjust the windowing. It might take several trials until we find the proper window.

SVI APPLIED TO NOISY LAND DATA

The SVI method is applied to data recorded over a shallow basin in East Africa, where the objective is to determine the topography of the shallow bedrock. The surface layer consisted of loose small clay particles and there was a persistent 5-20 kph wind noise and significant scattering at the near surface due to shallow volcanics. 240 vertical-component geophones were deployed along a 1.2 km line, with a geophone spacing of 5 m, and 120 shots were located next to every other geophone for a shot interval of 10 m. The shot consisted of a 200-lb accelerated-weight-drop source, and we used up to 30 stacks at each shot station. Even with this high number of shots per shot station, the stacked shot gathers were inundated with severe noise (see Figure 2(a)). The noise is largely due to the high level of wind noise (more than 10 km/hour) and the near-surface scattering.

To reduce this noise we tested three noise-reduction strategies: bandpass filtering, predictive error filtering, and SVI. We tested the performance of the predictive error filter (PEF) for diffreent filter lengths and prediction distances, and display the results for the optimal set of parameters. We also tested the bandpass filter for a range of different bandwidths and only display the filtered data for the optimal bandpass filter.

Figures 2(b), (c) and (d) depict the CSG after applying bandpass filtering, prediction error filtering, and SVI respectively. It is clear that the SVI traces in Figure 2(d) reveal far-offset arrivals that are clearly pickable. The dashed lines delineate the far-offset first arrivals picked from the SVI data. For comparison, these refractions are all unpickable to the naked eye in the band-pass filtered and PEF CSGs.

Reciprocity Test

To test the accuracy of the refraction arrivals in the SVI CSGs, the SVI procedure was applied to all of the CSGs

so that SVI shot gathers were constructed for every shot position. Figure 3 shows the traveltime picked from the data (a) before and (b) after SVI. We used a T/4 threshold filter, where picks were rejected if the reciprocal pair of traveltimes $\tau_{xx'}$ and $\tau_{x'x}$ did not agree to within a quarter of the dominant period T of the source wavelet; here, $\tau_{xx'}$ is the traveltime of a refraction event for a source at x and receiver at x'. The dark blue portions in the figures indicate rejected or unpicked traveltimes. Figure 3(b) shows that the vast majority of the SVI traveltimes satisfy the reciprocity condition.

Another sanity test is to compare a shot gather with a reasonable SNR, where the wind noise is not severe, to one reconstructed by the SVI procedure. Figures 4(a) and (b) depict a band-pass filtered CSG with a more tolerable SNR and the one reconstructed by SVI, respectively. The first arrival can be detected in Figure 4(a), and is marked by the dashed line. We surmise that the first-arrival traveltimes in both CSGs agree with one another to within $T/4$.

Traveltime Tomograms with SVI Data

The main benefit of SVI is that it provides many more pickable refractions in noisy data. As an example, Figure 3 depicts the traveltime matrix a) before and b) after applying SVI to the CSGs. The SVI method increased the number of invertible traveltimes by 21% compared to picking with the band-pass filtered data.

The increased number of picks provided by SVI enhances the extent and accuracy of the tomogram, as shown in Figure 5. An artifact is the apparent low-velocity zone shown in the tomogram constructed from the band-pass filtered data. Here, the velocity update is insufficient in the circled zone due to the paucity of reliable traveltime picks. In contrast, a continuous bedrock layer pops out in the SVI tomogram after we use more picks from the SVI data. This is the expected quartzite bedrock at around 5 km/s as observed in the bedrock outcrop at the far left of the survey.

LIMITATIONS OF SVI

The SVI procedure is not able to always get "something from almost nothing". It has the following limitations, which are illustrated by examples from the land data collected in East Africa.

1. Coherent linear noise might be inadvertently enhanced by SVI. To mitigate this problem, a stringent reciprocity test is required and the design of windows over a reasonable range of moveout velocities should be employed.

2. The theory of the SVI requires that the windowed refractions originate from the same interface. In this case, we assume all the far-offset first arrivals are the refractions from the bedrock, according to the geological reference. However, the assumption is violated if the far-offset first arrivals are from a deeper layer. As illustrated in Dong et al. (2006), common pair gathers should be used to check the validity of this assumption, and the events from each refractor are treated separately from one another. This also provides the opportunity to enhance refractions that are not necessarily first arrivals.

CONCLUSIONS

Supervirtual interferometry is applied to East Africa land data. It reconstructs far-offset refractions that are buried by severe noise. SVI significantly outperforms band-pass filtering and predictive-error filtering in generating pickable refractions.

ACKNOWLEDGMENTS

We thank the sponsors of the Center of Subsurface Imaging and Fluid Modeling (CSIM) at Kaust for their support.

REFERENCES

Al-Hagan, O., S. Hanafy, and G. Schuster, 2014, Iterative supervirtual refraction interferometry: Geophysics, **10**, 443–449.

Bharadwaj, P., G. T. Schuster, and I. Mallinson, 2012, Theory of supervirtual refraction interferometry: Geophysical Journal International, **288**, 263–273.

Bharadwaj, P., X. Wang, G. T. Schuster, and K. McInton, 2013, Increasing the number and signal-to-noise ratio of obs traces with super-virtual refraction interferometry and free surface multiples: Geophy.J.Int, **192**, 1070–1084.

Dong, S., J. Sheng, and G. T. Schuster, 2006, Theory and practice of refraction interferometry: SEG Expanded Abstracts, **25**, 3021–3025.

Mallinson, I., P. Bharadwaj, G. Schuster, and H. Jakubowicz, 2011, Enhanced refractor imaging by supervirtual interferometry: The Leading Edge, **30**, 546–550.

Morey, D. and G. Schuster, 1999, Palaeoseismicity of the oquirrh fault, utah from shallow seismic tomography: Geophys. J. Int., **138**.

Nichols, J., D. Mikesell, and K. van Wijk, 2010, Application of the virtual refraction to near-surface characterization at the Boise Hydrogeophysical Research Site: Geophys. Prospect., **58**, 1011–1022.

Sheriff, R. and L. Geldart, 1995, Exploration geophysics: Cambridge University Press.

Tarantola, A., 1984, Inversion of seismic reflection data in the acoustic approximation: Geophysics, **49**, 1259–1266.

Zhu, X., D. Sixta, and B. Angstam, 1992, Tomostatics: turning-ray tomography + static corrections: Leading Edge, **11**, 15–23.

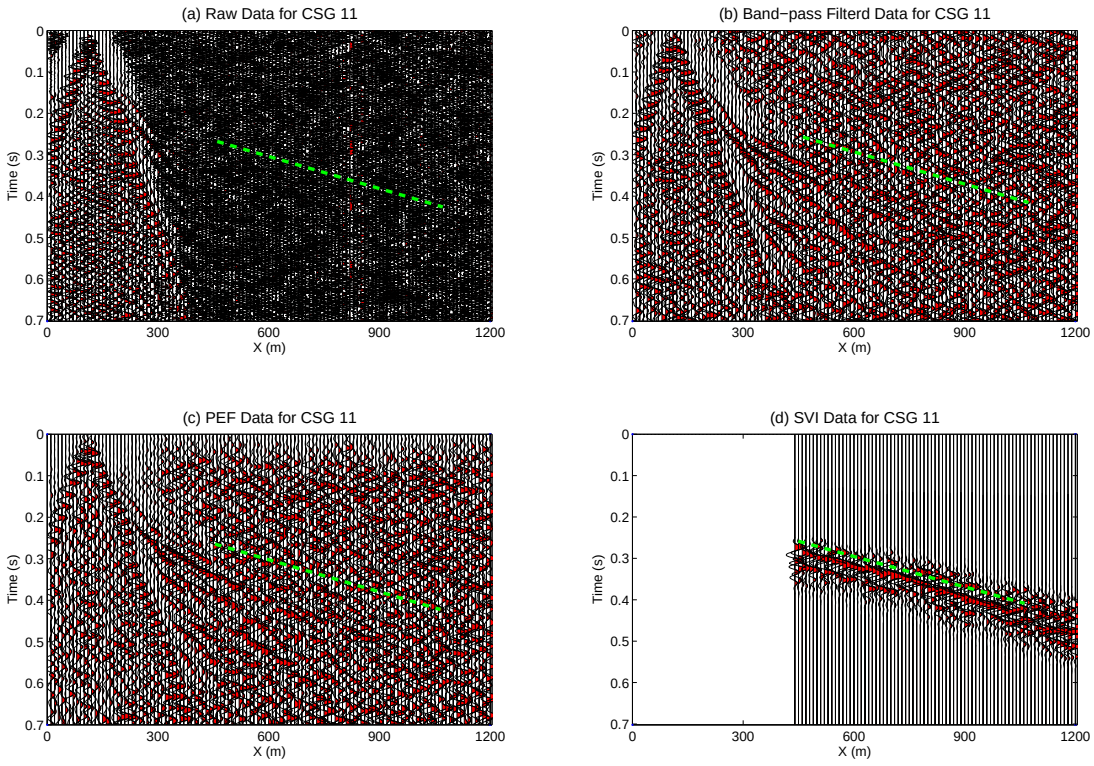

Figure 2: CSG 11 of (a) raw, (b) band-pass filtered, (c) PEF and (d) SVI data. The dashed lines approximately coincide with the first-arrival traveltimes picked from the SVI data. The far-offset first arrivals in (a), (b) and (c) are almost invisible.

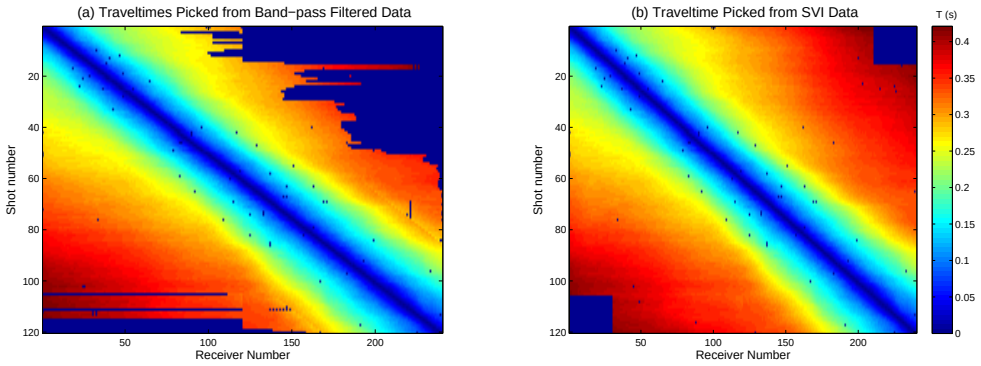

Figure 3: The traveltimes picked from (a) band-pass filtered and (b) SVI data. Rejected or unpickable traveltimes are marked as dark blue. SVI increases by 21% the number of pickable traces, which pass the reciprocity test.

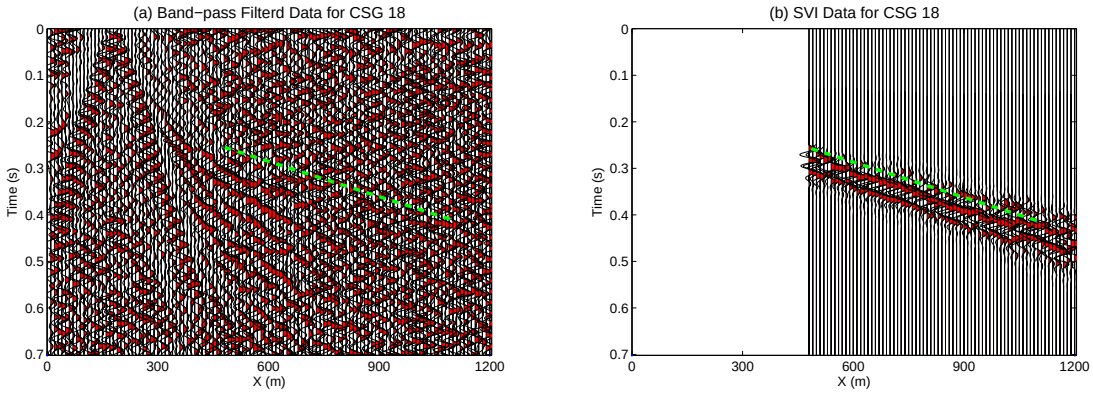

Figure 4: (a) Band-pass filtered and (b) SVI data of CSG18. The dashed lines are at the same positions in (a) and (b), indicating the first-arrival traveltimes.

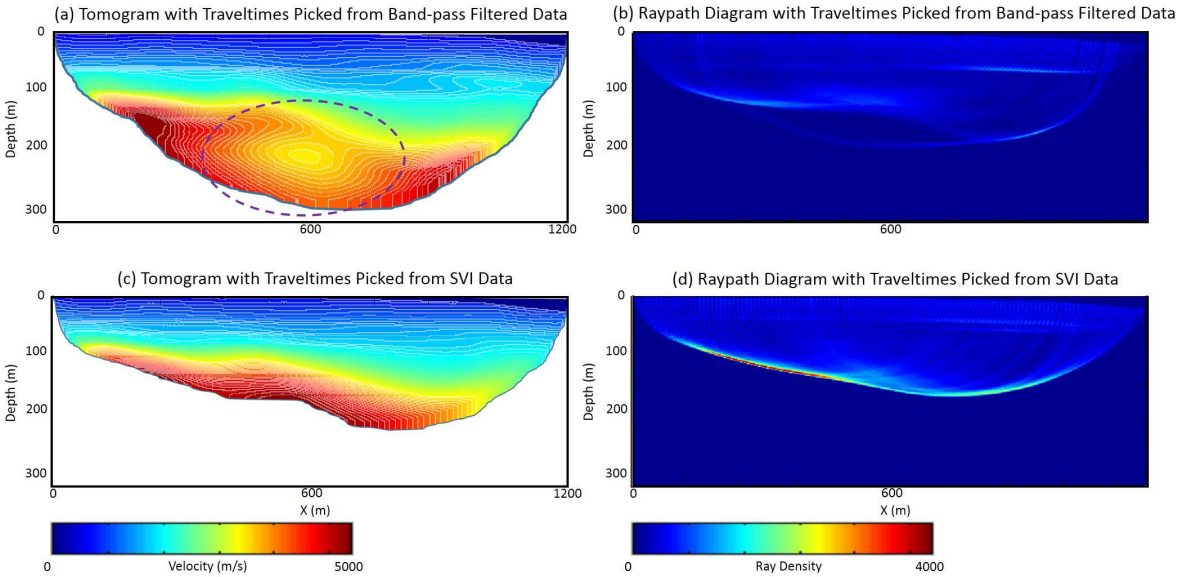

Figure 5: (a) and (b) are the tomogram and the raypath diagram inverted from the traveltimes picked in the band-pass filtered data, and (c) and (d) from SVI data. The low-velocity zone marked by the dashed oval in (a) is an artifact, and the ray paths in (b) are not concentrated to the bedrock layer, due to the paucity of far-offset traveltimes.